Sadeghi, Hosein; Hostikka, Simo; Fraga, Guilherme Crivelli; Bordbar, Hadi

Weighted-sum-of-gray-gases models for non-gray thermal radiation of hydrocarbon fuel vapors, CH4, CO and soot

Published in:
Fire Safety Journal

DOI:
10.1016/j.firesaf.2021.103420

Published: 01/10/2021

Document Version
Publisher's PDF, also known as Version of record

Fire Safety Journal 125 (2021) 103420

Contents lists available at ScienceDirect

Fire Safety Journal

journal homepage: www.elsevier.com/locate/firesaf

Weighted-sum-of-gray-gases models for non-gray thermal radiation of hydrocarbon fuel vapors, CH4, CO and soot

Hosein Sadeghi [a], Simo Hostikka [a], Guilherme Crivelli Fraga [b], Hadi Bordbar [a,*]

[a] Department of Civil Engineering, School of Engineering, Aalto University, P.O.B. 11000 Espoo, FI-00076, AALTO, Finland
[b] Department of Mechanical Engineering, Universidade Federal Do Rio Grande Do Sul, Porto Alegre, RS, Brazil

ARTICLE INFO

Keywords:
Spectral radiative heat transfer
Non-gray gas modeling
WSGG
Fuel vapor
Fire modeling

ABSTRACT

Using the high-resolution experimental spectral absorption coefficients of six fuel gases and the line by line absorption spectra of CO and CH_4 based on HITRAN and HITEMP spectral databases, in this paper, novel coefficients for weighted-sum-of-gray-gases (WSGG) model are presented for Heptane, Methane, Methanol, MMA, Propane, Propylene, Toluene, and CO. Moreover, for soot, the spectral absorption coefficients were calculated assuming Rayleigh regime implementing the complex index of refraction obtained from the correlations of Chang and Charalampopoulos. The presented WSGG models were coupled with those of literature for CO_2 and H_2O by means of the superposition method. The models were first validated in several one-dimensional benchmarks representing various levels of inhomogeneous conditions in temperature, gas concentration and soot loading. Then, the WSGG models were employed in solving a three-dimensional case representing a Heptane pool fire. Using the time averaged 3-D CFD profiles, the WSGG models solved the spectral radiative heat transfer exhibiting excellent agreement with the results of line by line calculations in terms of radiative heat flux and radiative heat source. Moreover, the emissivity charts were provided comparing the emissivity calculated by LBL calculations with those of the new WSGG models.

1. Introduction

Spectral radiative heat transfer in gaseous combustion is among the most challenging engineering problem to solve. The thermal radiation spectrum of gases may consist of millions of absorption lines closely located to each other that should be included in solving the integrated form of radiative transfer equation (RTE). Though the line-by-line integration method (LBL) [1] or narrow-band methods (NB) [2] can accurately solve gas spectral thermal radiation, due to their high computational costs, they have been mostly used to obtain the needed data to build other coarser models [3] and to provide benchmark solutions [4]. Therefore, using simplified spectral models in solving thermal radiation in engineering applications is inevitable.

The global models provide an accurate solution of the spectrally integrated RTE by interpreting the highly complex LBL absorption spectra of gases to smoother functions. These smoother functions are easier to integrate and therefore the final solution is computationally cheaper than LBL and NB solutions while accuracy is maintained at an acceptable level. The spectral-line-based WSGG (SLW) method [5,6], the absorption distribution function (ADF) method [7] and the full-spectrum correlated-*k* (FSCK) method [8] are the most important global models beside the weighted-sum-of-gray-gases (WSGG) model [9].

The WSGG model was first proposed by Hottel and Sarofim [10] in the framework of zone method [11,53] and Modest demonstrated its applicability to any RTE solution [9]. The WSGG model approximates the spectrally-integrated thermal radiation with a summation of RTE solutions of only a few gray gases each with a certain weight in the final summation. While the older WSGG models were based on gas total emissivity either measured experimentally [10] or calculated by the exponential wide band model (EWBM) [12], the more recent WSGG models are based on more accurate total emissivity databases calculated by LBL [3,13,14] or NB [15] calculations. They also support various modern combustion scenarios including oxygen-fired combustion [3,16], pressurized combustion [17,18], and micro-gravity combustion [18]. Most of the older WSGG models provided their parameters for single gases or for a few fixed molar fraction ratios of H_2O to CO_2 (i.e. $MR = Y_{H_2O}/Y_{CO_2}$). The parameters for gas mixtures were mostly obtained for $MR = 1$ approximating the combustion of oil and $MR = 2$ representing full combustion of Methane. For other molar fraction ratios, there is a need for interpolation between the model parameters

* Corresponding author.
E-mail address: hadi.bordbar@aalto.fi (H. Bordbar).

https://doi.org/10.1016/j.firesaf.2021.103420
Received 24 September 2020; Received in revised form 14 July 2021; Accepted 24 July 2021
Available online 28 July 2021

Nomenclature

a	Weight factor
b	Polynomial coefficient
C	Empirical constant of Rayleigh's theory
f_v	Volume fraction (-)
I	Total intensity (W/m^2 sr)
I_b	Blackbody intensity (W/(m^2 sr))
$I_{b\eta}$	Spectral Planck intensity (W/(m^2 sr cm^{-1}))
I_η	Spectral intensity (W/(m^2 sr cm^{-1}))
k_s	Imaginary part of refractive index
N_g	Number of gray gases
N_p	Order of polynomial function
n_s	Real part of refractive index
P	Total pressure (atm)
p	Partial pressure (atm)
q_r	Raduative heat flux (W/m^2)
r	Radius (m)
S_r	Radiative source term (W/m^3)
T	Temperature (K)
x	x position (m)
y	y position (m)
Y	Mole fraction (mol/mol)
w	The polynomial function in the scalar field Φ

Greek letters

δ	Relative error (%)
ε	Total emissivity
η	Wavenumber (cm^{-1})
κ	Absorption coefficient (m^{-1})
Φ	Arbitrary scalar field

Subscripts

j	Gray gas index
m	Mixture
n	Index of number
p	Pressure based
s	Soot
η	Spectral based

Abbreviations

1-D	One-dimensional
3-D	Three-dimensional
ADF	Absorption distribution function
FDS	Fire dynamics simulator
FG	Fuel gas
FSCK	Full-spectrum correlated-*k*-distribution
FSK	Full-spectrum *k*-distribution
GG	Gray gas
LBL	Line-by-line
MMA	Methyl methacrylate
RCSLW	Rank correlated spectral-line-based WSGG
RTE	Radiative transfer equation
SLW	Spectral-line-based WSGG
WSGG	Weighted-sum-of-gray-gases

which introduces remarkable error in non-homogeneous media. However, in recent years, several WSGG models [3,14,15] have been reported which include *MR* in their formulations and therefore provide much better accuracy. Depending on the accuracy of the total emissivity databases used in the development of the WSGG models, their treatment of non-homogeneity of media, and their implementation (number of gray gases, formulations, etc.), the WSGG models exhibited quite different computational performances in terms of accuracy and computational time. The comparative analysis of the performance of various WSGG models in different combustion scenarios can be found in many references including [19–22]. Kez et al. [20] compared the performance of several WSGG models, narrow-band correlated-*k* model, wide-band correlated-*k* model, and full-spectrum correlated-*k*-distribution model in modeling a three-dimensional oxy-fuel coal combustor. The error of the WSGG models in their study varied between 1% to 20% case by case. Considering the low computational costs of WSGG models, they concluded that the WSGG model is an efficient approach for engineering applications if appropriate parameters are applied. Nonetheless, without considering differences in computational costs, the FSCK model exhibited higher accuracy in general [20].

There are several studies reporting poorer accuracy of WSGG models compared to other global models. For instance, Pierrot et al. [23] compared the accuracy of several narrow-band and global models in predicting wall radiative heat flux of three slab problems representing emission-dominated and absorption-dominated problems. They reported up to 50% error in their WSGG model predictions while SLW and ADF models had deviations around 10%–20% with the same computational costs. Nonetheless, supporting absorption-dominated regime is challenging for other global models as well [24]. As WSGG models provide a quick way to calculate the emissivity of gas mixtures, they sometimes are used to obtain an effective mean absorption coefficient in gray gas modeling. For instance, Badger et al. [25] compared this kind of gray modeling with SLW models for an oxygen-fuel furnace. Not surprisingly, they reported considerable differences between the predictions of gray-WSGG modeling with those of RCSLW. In another recent study, Consalvi et al. [26] solved several turbulent axisymmetric jet diffusion flames at atmospheric and higher pressures using the FSCK [24] method, the RC-FSK [27] method, a WSGG model implementing the superposition approach for mixing the species [28] and a WSGG model obtained for two fixed *MR*s [17]. They reported slightly better accuracy for the FSCK method [24]. The CPU costs of the fixed *MR* WSGG model were the lowest while the CPU cost of *k*-distribution models for methane combustion was lower than the WSGG superposition model [28]. The computational cost and memory demand of RCSLW and FSCK methods have been recently improved by using the tabulated model parameters and some other techniques such as machine learning [29]. It is worth mentioning that the accuracy and computational costs of the SLW and FSCK methods can be tuned by changing the number of quadrature points/gray gases. This scalability is not feasible with WSGG models as they usually were developed for a fixed number of gray gases.

The main advantages of the WSGG model can be summarized as 1) simple formulation, 2) fairly good accuracy especially in coupled calculations and in emission-dominated systems such as combustors [19–22,30]), 3) low computational cost in the premixed format and 4) easy coding and implementation which make this model suitable for engineering calculations. On the other hand, its drawbacks can be listed as 1) mixing of different species which should be done by superposition which drastically increases the computational cost due to the high number of the required RTE solutions, 2) its dependency on total emissivity in the development stage which limits the model to certain ranges of pL and temperature and also reduces the accuracy of the model in absorption-dominated problems [23], 3) its lower accuracy compared to other global models [26,31], and 4) no chance of scalability as explained before.

It is worth noting that the thermal radiation in gaseous combustion is a compromise engineering problem [31]. It means that the choice of an appropriate model depends on the importance of spectral radiative heat

transfer in the overall accuracy of coupled CFD solution, the desired accuracy, and available computational resources. For instance, in soot-dominated combustion systems, one may not spend the computational resources for non-gray modeling as gray assumption may well approximate the medium. On the other hand, in micro-gravity conditions, due to the absence of convection, spectral thermal radiation is of a great importance and needs accurate treatment.

The WSGG model has been traditionally used for CO_2 and H_2O mixtures as the main combustion gas products participating in thermal radiation. Besides the WSGG models reported for the CO_2–H_2O mixture, there are only a few other WSGG models developed for other species, namely CO and soot [28,32]. The spectral radiative properties of soot clouds are derived by assuming very small soot particles following Rayleigh theory [1] which is applicable for spherical particles with diameters smaller than thermal radiation wavelengths. Based on experimental measurements, Chang and Charalampopoulos [33] proposed some correlations for calculating the spectral complex index of refraction of soot. Cassol et al. [28] presented a WSGG model for soot by assuming a wavenumber-independent refractive index for soot. CO is another radiative participating species in combustion products. Brittes et al. [34] presented their WSGG model for CO and compared its predictions with the results obtained by the RC-SLW model and line-by-line integration.

While CO_2, H_2O, and soot have the main contribution to radiative heat transfer in combustion spaces, the effect of other gases could be significant and should not be ignored [35]. For instance, Consalvi and Liu [36,37] showed that the concentration of vaporized fuel gases is remarkably high just above the pool surface in pool fires with mole fractions of about 0.3–0.8 for 34 kW and 176 kW methane pool fires, respectively [37]. Radiation contribution of the cold, fuel-rich region above the pools (or in front of burners) is particularly important as it can significantly affect radiation feedback to the pool which in turn affects the mass loss rate of the pool. Therefore, the impact of fuel gases on the thermal radiation of a flame is also important in providing accurate boundary conditions for models solving thermal radiation penetration within the liquid fuels, such as those reported in Refs. [38,39]. To date, the available spectral models for fuel vapors are limited to the Malkmus NB and NB *k*-distribution databases of Consalvi and Liu [2]. These databases were extracted from the experimental data of Wakatsuki [40] which is also used in the present work.

The present work provides WSGG models for Heptane (C_7H_{16}), Methane (CH_4), Methanol (CH_3OH), Propane (C_3H_8), Propylene (C_3H_6), MMA ($C_5H_8O_2$) and Toluene (C_7H_8). Moreover, we present new WSGG models for CO and soot and compare them with their previously published counterparts in Refs. [28,34,41]. The new WSGG models can be coupled with the previously published WSGG models for CO_2 and H_2O mixtures by applying the superposition approach [28,42].

Nevertheless, as mentioned before using the superposition approach may drastically increase the computational cost and therefore is not recommended for engineering calculations of large-scale combustion. The achieved models are verified using the well-known 1-D slab problem which provides enough flexibility to define different conditions. The applicability of the proposed models is further demonstrated in solving spectral radiation heat transfer in a large pool fire. This uncoupled radiation problem is constructed from the time-averaged CFD profiles of a pool fire [43,44]. The presented model can be used for studying some cases in fire research such as gasification process and controlled atmospheric cone calorimeter experiments where the contribution of fuel vapors in thermal radiation is significant.

2. Spectral absorption databases

Radiative heat transfer in participating media is described by the radiative transfer equation, which for emitting, absorbing and non-scattering media is given as

$$\frac{dI_\eta}{dx} = \kappa_\eta(x)[I_{b\eta}(x) - I_\eta(x)] \tag{1}$$

where η is the wavenumber, x is the position, κ_η is the spectral absorption coefficient and $I_{b\eta}$ is the spectral blackbody intensity. In this work, the high-resolution spectral absorption coefficients which are needed for generation of the new WSGG models' parameters and their validation were taken from different sources. Wakatsuki [40] measured the spectral absorption coefficients of Heptane, Methanol, MMA, Propane, Propylene, and Toluene using high-resolution FTIR at seven temperatures. The wavenumber ranged from 700 cm^{-1}–4000 cm^{-1} with a 0.5 cm^{-1} resolution. Here, these experimental data were interpolated and extrapolated whenever needed for a temperature range of 300K–1400K as proposed in Ref. [45]. Wakatsuki [40] showed that, for the above-mentioned six fuel gases, the contribution of the weak absorption lines outside the main absorption bands can be safely ignored.

We obtained the required high-resolution absorption spectra of H_2O, CO_2, CO and Methane by line-by-line calculations. Note that the spectra of H_2O and CO_2 were only needed to obtain the solutions of the 1-D and 3-D benchmarks. In the LBL calculations, HITEMP2010 database [46] was used for H_2O, CO_2 and CO and the absorption coefficients were generated for temperatures between 300K and 3000K. For Methane, the spectral absorption data were obtained from HITRAN2008 [47] for temperatures from 300K to 2450K. A uniform spectral resolution of 0.02 cm^{-1} was chosen for the spectrum from 150 cm^{-1}–15000 cm^{-1}. This resolution was reported to be optimum for LBL calculations in combustion applications [48]. More details of the performed LBL calculations of the present work can be found in Ref. [49].

Fig. 1 shows the line-by-line and experimental spectral absorption coefficients of different gas species at the temperature of 300K. It is seen in Fig. 1 that the absorption spectra of some fuel gases such as Methanol, MMA and Propane are in the same order of magnitude and also have the same position in the spectrum, which is due to their similar atomic structure. Accordingly, quite the same total emissivity can be expected for these gases followed by similar WSGG model's coefficients.

Soot is another species needed for radiation modeling of combustion

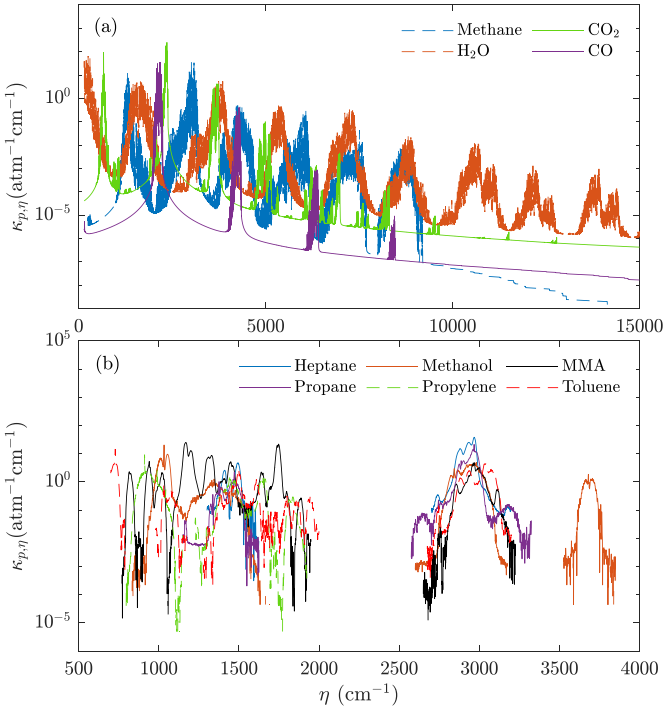

Fig. 1. Pressure-based absorption spectra of different gases at $T = 300$ K (a) line-by-line (b) experimental data.

systems. Assuming Rayleigh regime [1] for a cloud of sufficiently small soot particles, the spectral absorption coefficient of soot, $\kappa_{s\eta}$, is given by

$$\kappa_{s\eta} = C_\eta f_v \eta \tag{2}$$

where f_v is the volume fraction of soot. In general, spectral absorption coefficient of soot is calculated assuming either a linear or a non-linear dependence on the wavenumber. When $\kappa_{s\eta}$ is assumed to be a linear function, C_η is assumed to be constant ($= C$). Different fuel-dependent values of C have been reported in the literature, e.g., 4.0 for acetylene, 4.1 for methane flames, 4.9 for propane, 6.3 for oil combustion and 3.7–7.5 for coal combustion [28]. However, constant C is only a simplifying assumption, as C_η has been reported to vary with wavenumber [1]. Following Rayleigh's theory, C_η can be calculated as

$$C_\eta = \frac{36\pi n_s k_s}{(n_s^2 - k_s^2 + 2)^2 + 4\pi n_s^2 k_s^2} \tag{3}$$

where n_s and k_s are the real and imaginary parts of soot refractive index, respectively. Chang and Charalampopoulos [33] fitted two correlations over their experimental data of n_s and k_s as

$$n_s = 1.811 + 0.1263\ln(10^4/\eta) + 0.027\ln^2(10^4/\eta) + 0.0417\ln^3(10^4/\eta) \tag{4}$$

$$k_s = 0.5821 + 0.1213\ln(10^4/\eta) + 0.2309\ln^2(10^4/\eta) - 0.01\ln^3(10^4/\eta) \tag{5}$$

These equations have been widely used for calculating of soot spectral absorption coefficient [36,37]. Mean-Planck-weighted value of C_η provides a better understanding of the variations of C_η. It is calculated as

$$\overline{C}_\eta = \frac{\int_0^\infty I_{b\eta} C_\eta d\eta}{\int_0^\infty I_{b\eta} d\eta} \tag{6}$$

Fig. 2 shows the variation of mean-Planck-weighted C_η with temperature. As seen in Fig. 2, none of the mentioned constant values of C can accurately estimate C_η. Furthermore, Fig. 3 illustrates the soot spectral absorption coefficient for $f_v = 10^{-5}$ calculated using linear and non-linear functions. As seen, there is considerable differences in the spectral absorption coefficient of soot using the different constant values of C. Although Chang and Charalampopoulos [33] conducted their experiments for a propane burner, the constant $C = 4.9$ which was proposed for propane also can not exactly predict C_η. In this work, non-linear soot absorption coefficients were calculated using Eq. (2) and by employing Chang and Charalampopoulos's correlations, i.e. Eqs. (4) and (5).

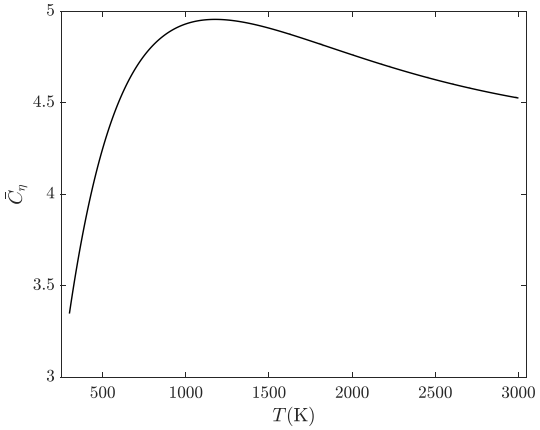

Fig. 2. Changes of mean Planck weighted values of C_η with temperature.

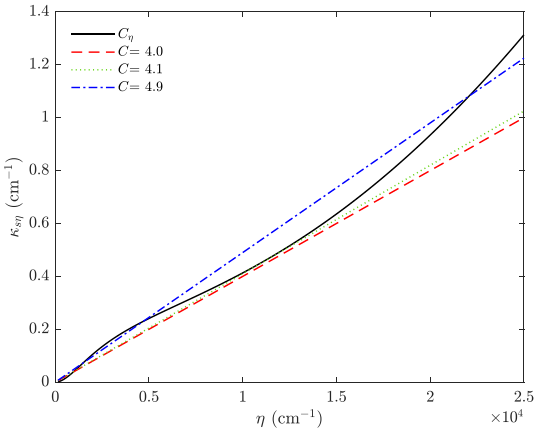

Fig. 3. Linear and non-linear spectral absorption coefficient of a soot cloud with $f_v = 10^{-5}$.

3. The WSGG model

3.1. WSGG coefficients for individual species

The WSGG model approximates the entire absorption spectrum with a few gray gases with absorption coefficient of κ_j and an additional gas representing transparent windows across the spectrum. The radiative transfer equation for each of the gray gases is written as

$$\frac{dI_j}{dx} = \kappa_j(x)\left[a_j(x) I_b(x) - I_j(x)\right] \tag{7}$$

where I_j is the intensity of the j-th gray gas and a_j is the weight factor expressing the fraction of blackbody energy at the temperature of the medium corresponding to the spectral regions whose contribution is approximated by κ_j.

The absorption coefficients of the gray gases and their weighting factors are obtained by fitting the total emissivity calculated by WSGG model (Eq. (9)) to the emissivity databases obtained from other sources. Using the high resolution spectra, total emissivity of a gas species is calculated as

$$\varepsilon = \frac{\int_0^\infty I_{b\eta}\left(1 - e^{-\kappa_{p\eta} pL}\right) d\eta}{\int_0^\infty I_{b\eta} d\eta} \tag{8}$$

where $\kappa_{p\eta}$ is the spectral pressure-based absorption coefficient, L is pathlength, and p is the partial pressure.

Total emissivity in WSGG model is calculated as

$$\varepsilon = \sum_{j=0}^{N_g} a_j(T_r)\left(1 - e^{-\kappa_{pj} pL}\right) \tag{9}$$

where N_g is the number of gray gases and $T_r = T/T_{ref}$, where $T_{ref} = 1400$ K is the reference temperature. The introduction of a reference temperature is useful for faster convergence and numerical stability of the fitting procedure and also for improving the accuracy of the polynomials by making the coefficients dimensionless [3,16,50]. An appropriate value for reference temperature is usually found by trial and error between the minimum and the maximum temperatures of interest for the model. Note that $j = 0$ represents the transparent part of the spectrum and therefore $\kappa_0 = 0$. The weight factor, $a_j(T)$, in this work is defined as

$$a_j(T) = \max\left(\sum_{n=0}^{N_p} b_{j,n} T_r^n, 0\right) \tag{10}$$

To ensure the conservation of energy, it is required that

$$\sum_{j=0}^{N_g} a_j(T) = 1 \tag{11}$$

The total emissivity is calculated by LBL integration in Eq. (8) for discrete sets of pL and T. Fitting Eq. (9) to the LBL-based emissivity databases, the κ_{pj} and $b_{j,n}$ are obtained. In the present work, the LBL emissivity databases are obtained for ten pLs chosen in the range of $0.01 \leq pL \leq 10$ atm.m. The valid practical temperature range can be different for different species. For Heptane, Methanol, MMA, Propane, Propylene and Toluene, the LBL-based emissivity is calculated for 23 evenly spaced temperatures between $300\text{K} \leq T \leq 1400\text{K}$. For CO, the coefficients were generated for 55 evenly spaced temperatures in the range of $300\text{K} \leq T \leq 3000\text{K}$ while they were calculated for Methane for 44 evenly spaced

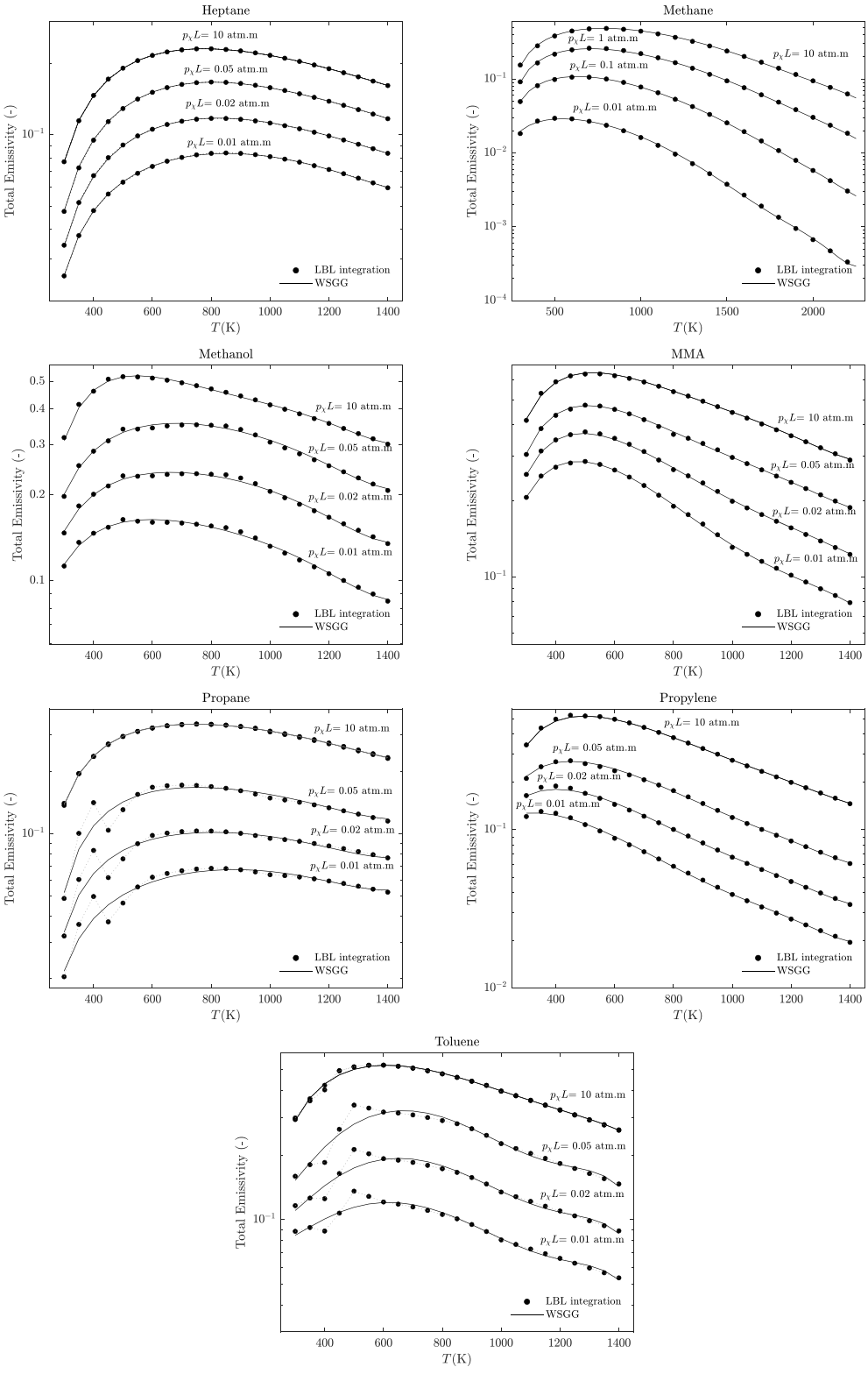

Fig. 4. Comparison of the total emissivity calculated by the LBL integration and the present WSGG model for the fuel gases.

temperatures in the range of 300K $\leq T \leq$ 2450K.

Although there is no limitation for the number of gray gases, a lower number naturally leads to lower computational cost, which is one of the main objectives of engineering models. Several studies have examined the number of the gray gases. Hottel and Sarofim [10] reported that in some cases, one gray gas and one transparent gas are enough to represent the spectrum. Brittes et al. [34] reported that increasing the number of gray gases more than four did not cause a noticeable change in the results. To date, numerous studies have investigated WSGG model employing 4 gray gases and one transparent gas with fine accuracies, for instance in Refs. [3,15,16,28,34,51]. Based on these observations, in the present study, WSGG coefficients were calculated by using 4 gray gases and one transparent gas, i.e. $N_g = 4$, and a fifth-order polynomial was employed for the weight factor $a_j(T)$, i.e. $N_p = 5$.

In the fitting procedure, the Least Square method was used as the optimization method in MATLAB software and the constraints of $\kappa_{pj} > 0$, $a_j(T) > 0$ and $\sum_{j=0}^{N_g} a_j(T) = 1$ were applied to the calculations. The calculated WSGG coefficients for Heptane, Methanol, MMA, Propane, Propylene, Toluene, Methane, CO and soot are provided in Appendix A. Fig. 4 compares the total emissivity calculated by LBL integration and by the WSGG model using the obtained coefficients for the seven fuel gases.

A comparison between total emissivity calculated by the LBL integration and by present WSGG model and the results of Brittes et al. [34] for CO is shown in Fig. 5. As it can be seen, the fifth-order polynomial weight factor, $a_j(T)$, in Eq. (9) is able to estimate the LBL total emissivities more accurately than the fourth-order weight factor used in Ref. [34] and can reach almost exact total emissivities through Eq. (9).

Comparisons with previously reported WSGG coefficients are also made for soot. Cassol et al. [28] proposed soot WSGG coefficients using the linear approximation of spectral absorption coefficient (i.e., $C_\eta = C$) for 400K $\leq T \leq$ 2500K. In the present work, the WSGG coefficients of soot were reported based on the non-linear dependency of soot absorption coefficient to wavenumber following the Chang and Charalampopoulos correlations [33]. The present model also covers a wider temperature range of 300K $\leq T \leq$ 3000K, which makes the coefficients applicable to a wider range of applications. Fig. 6 compares the emissivities calculated by the present WSGG model, Cassol et al. WSGG model [28] and Coelho et al. WSGG model [41] with those of the LBL integration using the Chang and Charalampopoulos correlations in Rayleigh theory. As Fig. 6 illustrates, Cassol's models are accompanied by considerable errors. The emissivity charts shown in Figs. 5 and 6 confirm that the present WSGG models approximate the exact total emissivity databases well.

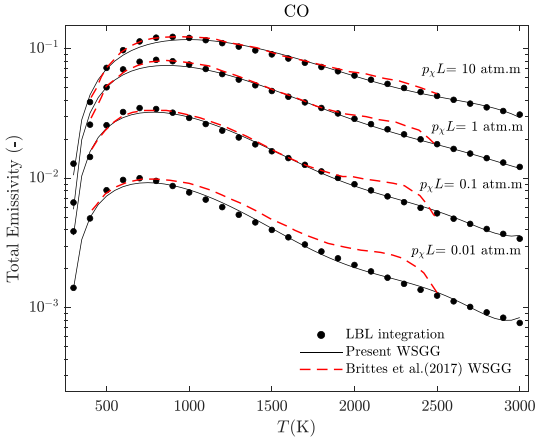

Fig. 5. Comparison of the total emissivity of CO calculated by the LBL integration, the present WSGG model and the WSGG model of Brittes et al. [34].

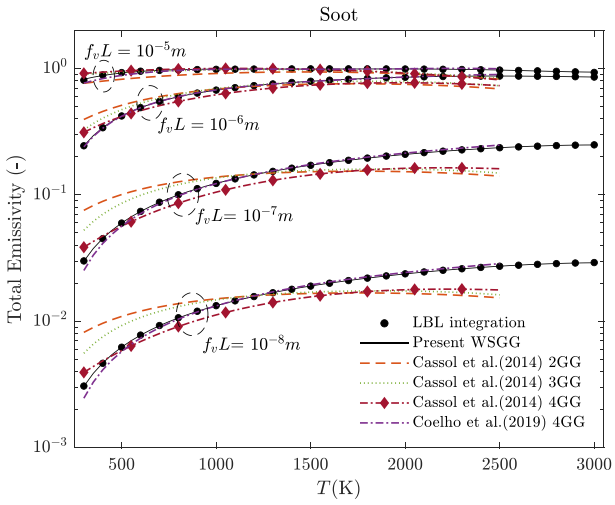

Fig. 6. Comparison of the total emissivity of soot calculated by the LBL integration, the present WSGG model, WSGG models of Cassol et al. [28] and Coelho et al. [41].

3.2. Superposition method in solving RTE for a gas mixture

Implementing the WSGG models, the RTE (Eq. (7)) can be solved using the given weight factors and the gray gas absorption coefficients. The present research aims to study the fuel-rich gas layer of a flame where the concentration of the combustion products can not be considered constant. In this case, the WSGG models of different species can be combined via the *Superposition Method* [28,42]. In the superposition method, it is assumed that the weight factor of the gray gas j, a_j, represents the probability that the blackbody energy at the gas temperature in position x is emitted in the wavenumbers of the spectrum where the absorption coefficient of the gray gas j is κ_{pj}. Hence, the weight factor for a gas mixture of a given combination of gray gases is equal to the cross product of their respective weight factors. Accordingly, for a mixture of n components, the absorption coefficient and weight factor of different RTE solutions are given by

$$\kappa_{m,j_m}(x) = \kappa_{1,j_1}(x) + \kappa_{2,j_2}(x) + \cdots + \kappa_{n,j_n}(x) \tag{12}$$

$$a_{m,j_m}(x) = a_{1,j_1}(x) \times a_{2,j_2}(x) \times \cdots \times a_{n,j_n}(x) \tag{13}$$

where index m refers to the mixture and $0 < j_m < N_{g_m}$. Therefore, if each non-gray component is modeled with N_g gray gases, the total number of gray gases of the mixture will be

$$N_{g_m} = (N_{g_1} + 1) \times (N_{g_2} + 1) \times \cdots \times (N_{g_n} + 1) \tag{14}$$

It is worth noting that in this formulation, the transparent windows of each component must be considered. Thus $0 < j < N_{g_m}$ and consequently, the number of gray gases of a component is equal to $N_{g_m} + 1$ in Eq. (14). Though the superposition method provides a way for treating mixtures with the WSGG models, it considerably increases the number of the required RTE solutions and CPU cost of the calculations. Therefore, this approach may not be affordable for large-scale engineering applications.

Calculation of the weight factors in the superposition method is in line with an assumption equivalently used in k-distribution method. It states that the absorption spectra of the individual species are statistically uncorrelated and therefore the product of the quadrature weights are used [52]. The superposition method is applicable to any mixture of gases. However, due to continuity of absorption spectrum of soot, the transparent gas is not needed to be considered for soot, so $1 < j_s < N_{g_s}$.

Finally, it is important to note that, while the formulation described in this section has historically been named the superposition method in

the framework of the WSGG model (see, e.g. [28,51]), similar approaches have been applied for the treatment of mixtures of participating species with other global models, where they receive different names. For instance, in the SLW model, the method is called the Multiple Integration method (or the Double Integration method [42]), whereas the name superposition method denotes a different approach for dealing with mixtures.

4. Results and discussion

Besides the model verification through the emissivity charts, to further validate the new WSGG models, the radiation heat transfer is solved in several 1-D benchmarks representing various levels of complexity and heterogeneity in thermal conditions of participating media which consist of fuel gases, combustion gases and soot. The benchmarks represent one-dimensional media bounded by two parallel black walls at constant temperatures as typically used in the literature of gas spectral radiation, e.g., [8,18,28]. Fig. 7 schematically shows the 1-D slab problems studied in this work. As described in [9], the WSGG model can be used with any method to integrate the RTE over the spatial domain. The Discrete Ordinates (DO) method was employed to solve the radiative heat transfer. In this work, the 8th-order approximation was employed. Here, the RTE in the framework of discrete ordinates method is written as

$$\mu_l \frac{dI^+_{\eta,l}}{dx} = \kappa_{m,\eta}(x)\left[I_{b\eta}(x) - I^+_{\eta,l}(x)\right] \tag{15}$$

$$-\mu_l \frac{dI^-_{\eta,l}}{dx} = \kappa_{m,\eta}(x)\left[I_{b\eta}(x) - I^-_{\eta,l}(x)\right] \tag{16}$$

where $\mu_l = \cos(\theta_l)$ is the direction cosine of angle l, and $I^+_{\eta,l}$ and $I^-_{\eta,l}$ are the spectral radiative intensities propagating along direction l in the forward and backward directions, respectively (see Fig. 7). Solving Eqs. (15) and (16) for all the directions and integrating over the spectrum, the radiative heat flux, q_r, and radiative source term, S_r, are obtained as

$$q_r(x) = \sum_{l=1}^{L} \int_\eta 2\pi w_l \mu_l \left[I^+_{\eta,l}(x) - I^-_{\eta,l}(x)\right] d\eta \tag{17}$$

$$S_r(x) = \sum_{l=1}^{L} \int_\eta 2\pi \kappa_\eta(x) w_l \left[I^+_{\eta,l}(x) + I^-_{\eta,l}(x)\right] - 4\pi\kappa_\eta(x) w_l I_{b\eta}(x) d\eta \tag{18}$$

where w_l is the quadrature weight for direction l. Applying the discrete ordinates method to Eq. (7), the RTE is obtained as

$$\mu_l \frac{dI^+_{m_j,l}}{dx} = \kappa_{m_j}(x)\left[a_{m_j}(x) I_b(x) - I^+_{m_j,l}(x)\right] \tag{19}$$

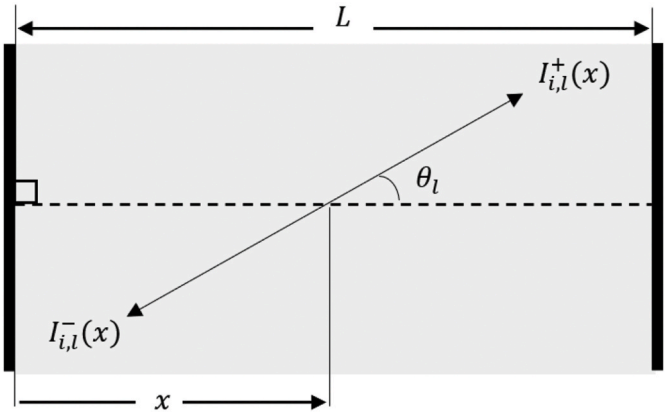

Fig. 7. Schematic of the one-dimensional medium slab.

$$-\mu_l \frac{dI^-_{m_j,l}}{dx} = \kappa_{m_j}(x)\left[a_{m_j}(x) I_b(x) - I^-_{m_j,l}(x)\right] \tag{20}$$

The radiative heat flux and source term in the frame work of WSGG model are obtained as

$$q_r(x) = \sum_{l=1}^{L} \sum_{j=0}^{N_{gm}} 2\pi w_l \mu_l \left[I^+_{m_j,l}(x) - I^-_{m_j,l}(x)\right] \tag{21}$$

$$S_r(x) = \sum_{l=0}^{L} \sum_{j=0}^{N_{gm}} 2\pi\kappa_{m_j}(x) w_l \left[I^+_{m_j,l}(x) + I^-_{m_j,l}(x)\right] - 4\pi\kappa_{m_j}(x) w_l a_{m_j}(x) I_b(x) \tag{22}$$

where $I^+_{m_j,l}$ and $I^-_{m_j,l}$ have the same definition as spectral intensities, but for gray gas j of the mixture.

To solve the RTE equation, the 1st order upwind discretization scheme was employed. Dirichlet boundary conditions equal to Planck's function at the wall temperature were assumed on the left and right boundaries. After performing a mesh independence analysis, the numerical domain was divided into 100 equal-sized elements. The total pressure of the system was set to P = 1atm. To evaluate the WSGG models, five cases with various level of complexity in temperature and species profiles are considered as introduced in Table 1. To obtain the benchmark solutions, whenever needed, the experimental absorption spectra of fuel gases with the resolution of 0.5 cm^{-1} were adapted to the resolution of 0.02 cm^{-1} used in LBL absorption spectra of CO, CH_4, CO_2 and H_2O.

The accuracy of the solutions was assessed by observing the relative error of the radiative heat flux and radiative heat source obtained by the WSGG model as

$$\delta(x) = \frac{|\varphi_{WSGG}(x) - \varphi_{LBL}(x)|}{max(|\varphi_{LBL}(x)|)} \times 100\% \tag{23}$$

where $\varphi_{WSGG}(x)$ and $\varphi_{LBL}(x)$ are representatives of radiative heat flux or radiative heat source obtained from WSGG model and LBL integration in position x, respectively. In the following, the benchmarking process starts from a simple case with only one active species with a fixed homogeneous concentration and temperature and gets more complex case by case to the test case 5. To couple the novel WSGG models with those previously developed for H_2O and CO_2, the coefficients reported in Ref. [51] were utilized wherever needed as separate gases. In Table 1, FG stands for fuel gas.

Table 1
1-D test cases.

Case	κ ($atm^{-1}m^{-1}$)	T (K)	Fuel	Radiatively active components	Mole/Volume fraction (mol/mol) (m^3/m^3)
1	$\kappa(\eta)$	1000	–	Soot	$f_v = 10^{-5}$
2	$\kappa(\eta)$	1000	Methanol, MMA, Propane	Fuel gas, H_2O, CO_2, CO, soot	$Y_{FG} = 0.04$, $Y_{H_2O} = 0.1$, $Y_{CO_2} = 0.05$, $Y_{CO} = 0.04$, $f_v = 10^{-7}$
3	$\kappa(\eta, x)$	$T(x)$	Heptane, Propylene, Toluene	Fuel gas, H_2O, CO_2, CO, soot	$Y_{FG} = 0.04$, $Y_{H_2O} = 0.1$, $Y_{CO_2} = 0.05$, $Y_{CO} = 0.04$, $f_v = 10^{-7}$
4	$\kappa(\eta, x)$	$T(x)$	Methane	Fuel gas, H_2O, CO_2	$Y_{FG}(x)$, $Y_{H_2O}(x)$, $Y_{CO_2}(x)$
5	$\kappa(\eta, x)$	$T(x)$	Propane, Propylene, Toluene	Fuel gas, H_2O, CO_2, CO, soot	$Y_{FG}(x)$, $Y_{H_2O}(x)$, $Y_{CO_2}(x)$, $Y_{CO}(x)$, $f_v(x)$

4.1. One-dimensional verification

Test case 1: The first case was designed to evaluate the present WSGG model for soot. Here, the domain contains only soot as a radiatively active medium with $f_v = 10^{-5}$ at $T = 1000$K and the boundaries, located at $x = 0$ m and $x = 1$ m, are at $T = 400$K. In this test case, the soot WSGG models of Cassol et al. [28], using two, three and 4 gray gases (GG), and Coelho et al. [41] are also included in the comparison. Additionally, a gray gas calculation based on Planck-mean absorption coefficient was done using the soot spectral absorption coefficients obtained from Chang and Charalampopoulos correlations (i.e. Eqs. (2)–(5)).

Fig. 8 shows the comparison between the WSGG models, gray gas model and two LBL calculations: one based on the Chang and Charalampopoulos correlations [33] and another using linear approximation with $C = 4.1$. As seen in Fig. 8, the present WSGG model for soot finely estimates the results obtained by the LBL calculations of this work. The Cassol's model has deviations and the Coelho's model works fine. Note that the present soot WSGG model is applicable for a wider temperature range than the Coelho's model. The average and maximum values of relative errors of each model are presented in Table 2.

To provide an easy way for gray calculation of soot, Eq. (24) was fitted to the data of volume-based Planck-mean absorption coefficient of soot shown in Fig. 9. The spectral absorption coefficient calculated by Eq. (2) was used to derive this correlation as

$$\bar{\kappa}_s = a\,T^3 + b\,T^2 + c\,T + d \tag{24}$$

where $a = 2.156 \times 10^{-5}$ K^{-3}, $b = -0.2889$ K^{-2}, $c = 1804$ K^{-1} and $d = -2.012 \times 10^{5}$ K.

Test case 2: In the second case, a full combustion scenario including fuel gas, H_2O, CO_2, CO and soot was studied. In this case, the mixture temperature was set to $T = 1000$K and mole fraction of the components were $Y_{FG} = 0.04$, $Y_{H_2O} = 0.1$, $Y_{CO_2} = 0.05$, $Y_{CO} = 0.04$ and $f_v = 10^{-7}$. On top of the WSGG models reported here, those of Ref. [51] were employed for H_2O and CO_2 and the superposition method discussed in section 3.2 was applied to support simulation of the mixture of different species. Fig. 10 compares the results of LBL integration and the present WSGG models for different fuel gases. As seen, the profiles of radiative heat flux and heat source calculated using the present WSGG correlations implemented in the superposition method are in a good agreement with those of LBL calculations. The results obtained from the line-by-line integration show very close values for MMA and Methanol due to their similar absorption spectra, as shown in Fig. 1.

Test case 3: This case represents the full combustion scenario with the inhomogeneous temperature profile of Eq. (25). Fig. 11 shows the profiles employed in this case as well as cases 4 and 5. A comparison between the results of the present WSGG model and the LBL integration for this case is shown in Fig. 12.

Table 2
The maximum and average relative errors and the CPU time.

Case	N_g(a)	δ_{max}(%)		$\delta_{average}$(%)		CPU time
		q_r	S_r	q_r	S_r	
1	1	15.43	48.51	13.58	18.30	1(b)
	2 ([28])	10.22	11.59	3.39	1.98	1.9
	3 ([28])	3.93	9.41	1.56	1.48	2.4
	4 ([28])	7.98	17.01	3.62	2.12	2.9
	4 ([41])	0.57	17.26	0.13	0.26	2.9
	4	0.85	16.49	0.13	0.29	2.9
2	2500	3.03	2.96	1.34	1.22	1076
3	2500	5.13	6.44	2.93	3.81	1076
4	25 ([13])	4.39	8.28	1.95	3.93	12.9
	25 ([3])	5.11	5.32	1.61	3.40	12.9
	125	5.29	3.63	1.10	1.85	62.5
5	2500	5.66	3.12	1.51	1.74	1076
3-D	500	5.50	2.01	0.56	0.08	225(c)

(a) N_g = number of required RTE solutions.
(b) $t_{LBL}/t_{GG} = 90909$.
(c) $t_{LBL}/t_{GG} = 52631$.

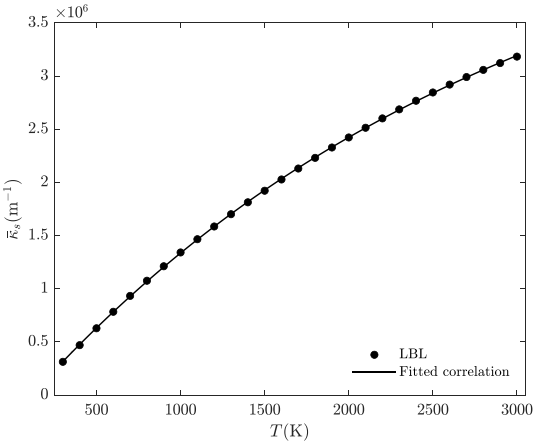

Fig. 9. The Planck-mean absorption coefficient of soot calculated by the LBL integration and Eq. (24) at $f_v = 1$.

$$T(x) = 300K + 1100K\,sin^2(\pi x) \tag{25}$$

Test case 4: In the case 4, a complete combustion of Methane was modeled which includes fuel gas, H_2O and CO_2 as the combustion products. If there is enough oxygen for combustion, Methane naturally undergoes complete combustion and, therefore, the mixture of gaseous

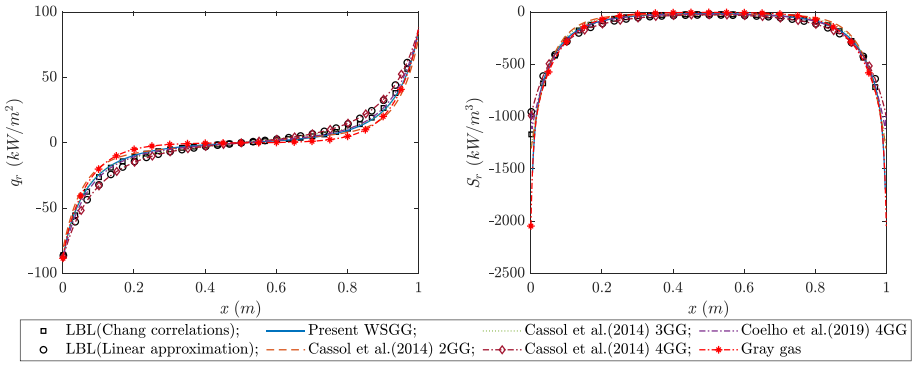

Fig. 8. Results of the test case 1.

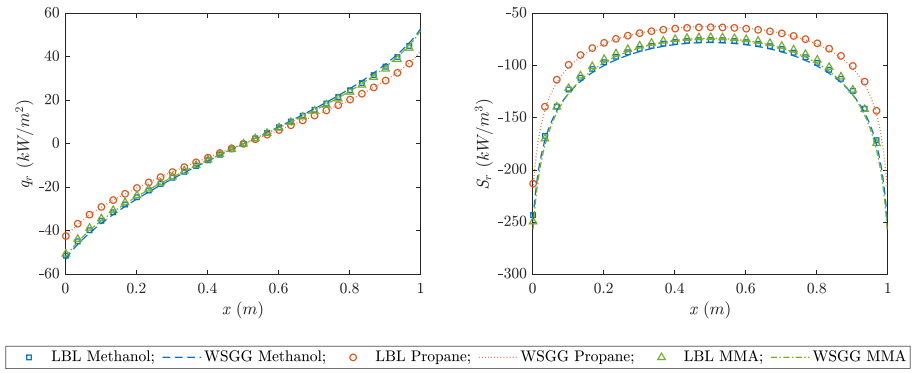

Fig. 10. Results of the test case 2.

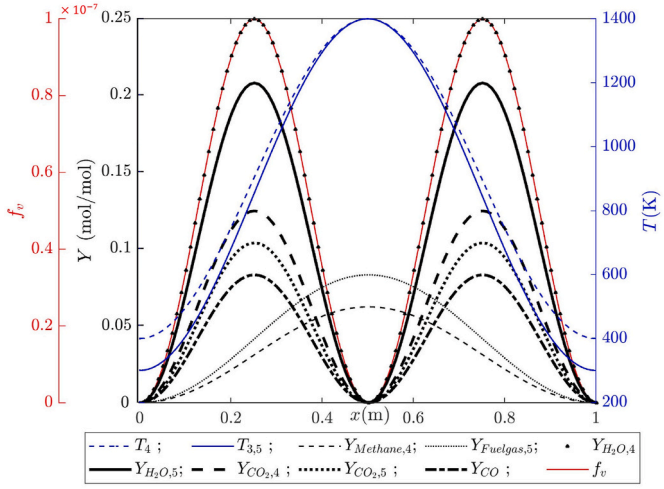

Fig. 11. The profiles of temperature, mole fraction of species and soot volume fraction used in different test cases specified as subscripts. The indices indicate the case number.

products is only composed of Methane, H_2O and CO_2. In this case, the WSGG coefficients for Methane obtained in this work and the coefficients for H_2O and CO_2 reported in Ref. [51] were used. A way to reduce the number of RTE solutions in the superposition approach is to use the WSGG models proposed for the H_2O–CO_2 mixture. To study how it may affect the accuracy and CPU costs of the calculations, we also solved this test case by using the reported WSGG coefficients of [3,13] for H_2O–CO_2 mixture. For the present WSGG model where the mixture consists of the three species, the superposition method needed 125 gray gases (i.e. RTE solutions). Since the coefficients in Refs. [3,13] were calculated for the mixture of the H_2O and CO_2 as a single gas mixture, 25 gray gases were required when the present WSGG model of Methane is coupled with these models. A comparison between the results obtained from the WSGG models and LBL integration can be found in Fig. 13 with the relative errors reported in Table 2. Temperature of the medium and mole fractions of Methane, H_2O and CO_2 are defined in Eqs. (26)–(29), respectively. The considered profiles for temperature and species concentrations are shown in Fig. 11.

$$T(x) = 400K + 1000K\ sin^2(\pi x) \tag{26}$$

$$Y_{Methane}(x) = 0.03\ sin^2(\pi x) \tag{27}$$

$$Y_{H_2O}(x) = 0.12\ sin^2(2\pi x) \tag{28}$$

$$Y_{CO_2}(x) = 0.06\ sin^2(2\pi x) \tag{29}$$

The results of WSGG modeling shown in Fig. 13 agree well with those of the LBL integration. Moreover, it can be seen that coupling the model with the WSGG models developed for the mixture of H_2O–CO_2 is more sensible than coupling it with the WSGG models developed for single gases. This is because the former needs less RTE solutions and consequently shorter CPU time, while no distinguishable privilege in accuracy was seen between these two modeling options.

Test case 5: This case examines the performance of the present WSGG model for the full combustion of Propane, Propylene or Toluene where H_2O, CO_2, CO and soot exist in the medium. The considered profiles for temperature and mole fractions of fuel gas, water vapor, CO_2, CO, and soot are given in Eqs. (30)–(35), respectively, and they can be found in Fig. 11. If the WSGG models for H_2O and CO_2 in Ref. [51] get implemented, 2500 gray gases plus one transparent gas would be needed for the WSGG model of this case.

$$T(x) = 300K + 1100K\ sin^2(\pi x) \tag{30}$$

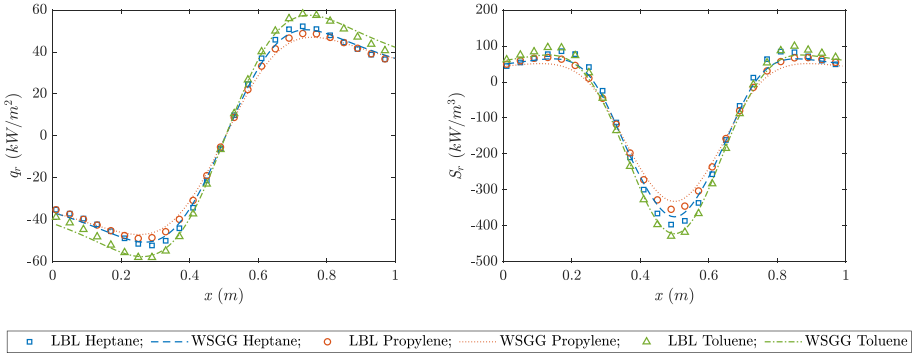

Fig. 12. Results of the test case 3.

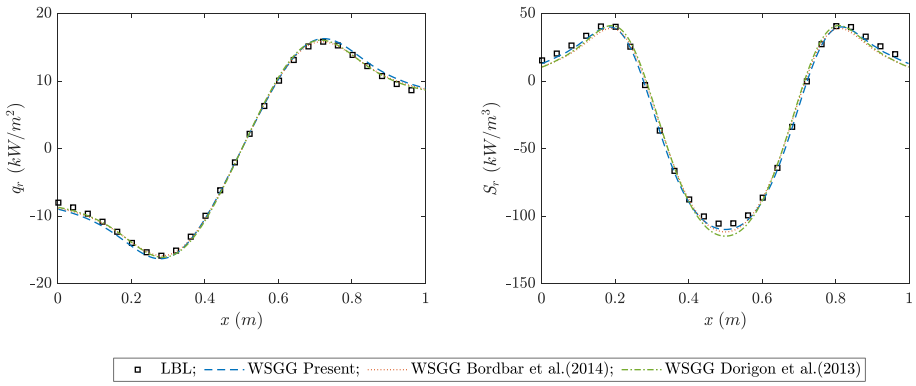

Fig. 13. Results of the test case 4.

$$Y_{FG}(x) = 0.04\ sin^2(\pi x) \tag{31}$$

$$Y_{H_2O}(x) = 0.1\ sin^2(2\pi x) \tag{32}$$

$$Y_{CO_2}(x) = 0.05\ sin^2(2\pi x) \tag{33}$$

$$Y_{CO}(x) = 0.04\ sin^2(2\pi x) \tag{34}$$

$$f_v(x) = 10^{-7}\ sin^2(2\pi x) \tag{35}$$

Fig. 14 illustrates the results from the calculations using the WSGG models and the LBL integration. As the absorption spectra of these fuel gases are close, their results of LBL integration are close.

4.2. Three-dimensional validation

In addition to the one-dimensional cases, a three-dimensional uncoupled thermal radiation problem was solved using line-by-line integration and WSGG modeling. This case represents a 2m-diameter Heptane pool fire based on the study of Bordbar and Hostikka [43] in which they modeled the pool fire with Fire Dynamics Simulator (FDS) in order to study the spectral intensity of the fire. They later further developed their detailed spectral analysis to several Kerosene pool fires [44]. Here we used the time averaged CFD profiles of their heptane pool fire [43] to define a 3-D validation case. The computational domain was a $2.4 \times 2.4 \times 4.75\ m^3$ enclosure, with boundaries located at $-1.2\ m$ and $1.2\ m$ along the x and y directions, and at $0.25\ m$ and $5.0\ m$ along direction z. The surface of the pool fire assumed to lie at $(x, y, z) = (0, 0, 0)$; further increasing the domain size did not lead to appreciable changes in the results for the radiation field near the flame. To all boundaries except the top one (i.e., the one at $z = 5.0\ m$), an open boundary condition to an atmospheric environment was imposed. Because the medium temperature is still fairly larger than the ambient temperature near the top bounding surface, the top boundary was taken as a black wall at $T =$ 473K, which is approximately the average medium temperature (computed from Eqs. (36) and (38) below) at $z = 5.0\ m$.

The species of Heptane, H_2O, CO_2, CO and soot are the radiative participating species and their spatial distributions were determined by fitting the time-averaged CFD results of the scalars of interest obtained by Bordbar and Hostikka [43]. The resulting profiles are as

$$\Phi_{H_2O,CO_2,CO,soot,T}(r,z) = \max\left(\sum_{j=1}^{4} w_j(r)(1-e^{-c_j z}), l\right) \tag{36}$$

$$\Phi_{Heptane}(r,z) = \min\left(\max\left(\sum_{j=1}^{4} w_j(r)(1-e^{-c_j z}), l\right), 1\right) \tag{37}$$

where

$$w_j(r) = \sum_{n=0}^{4} b_{j,n} r^n\ ; \quad r = \min(\sqrt{x^2+y^2}, 1.2m) \tag{38}$$

In Eq. (36), Φ represents temperature or species' concentrations. The constant l was used for bounding the imposed profiles, with $l = 0$ for calculating species' concentrations and $l = 293.15K$ for temperature profile. The values of c_j and $b_{j,n}$ coefficients depending on the scalar Φ are reported in the supplementary materials of this work.

The 3-D radiative transfer calculations were carried out in a modified version of the FDS solver, in which both the WSGG model with the correlations developed in the present paper together with the model of Ref. [3] for H_2O–CO_2 mixture and the LBL integration have been introduced. Details on this implementation can be found in [4]. Here, the superposition method was used in the WSGG modeling to mix the species. FDS uses the finite volume method to solve the RTE. A total of forty-eight finite solid angles was set for the angular discretization, while the spatial discretization was achieved with a $48 \times 48 \times 95$, uniformly-spaced grid cells mesh, which yields volume cells with a

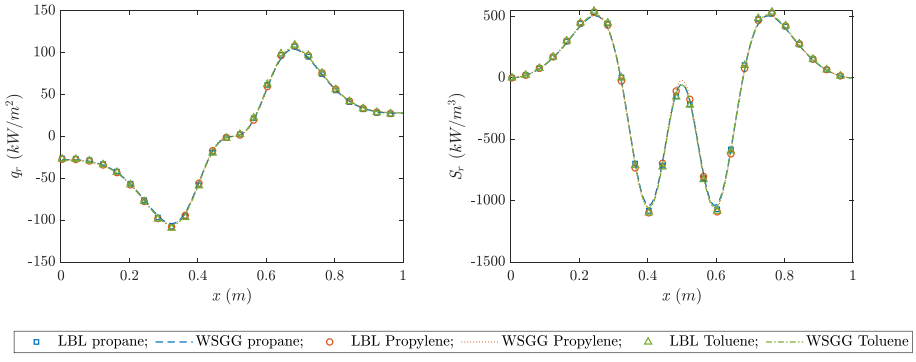

Fig. 14. Results of the test case 5.

characteristic size of 5 cm. A careful mesh size analysis showed that further refinement of the angular and spatial meshes has no significant effect on the results.

Fig. 15 illustrates the scalar field of radiative heat source at $y = 0$ obtained from the LBL integration and the WSGG modeling. According to Fig. 15, the hot gas at the flame front and the tip of the flame have the highest emission (i.e., $S_r < 0$), and surrounding the exterior of the flame there is a small region of lower temperatures in which absorption dominates. Comparing the two scalar fields, we can see that the WSGG modeling is in a satisfactory agreement with LBL integration. To corroborate this, Fig. 16 compares radiative heat source at the centerline of the pool, and radiative heat flux at surface of the pool and a side boundary in more details. Table 2 reports the errors concerning the WSGG model and the computational cost compared to the gray gas assumption.

4.3. CPU time analysis

The main advantage of the global models including WSGG model is their good accuracy and low computational costs. However, applying the superposition method demands a higher number of RTE solutions compared to the conventional WSGG models so, assessing the computational cost of the present models is of great importance. Among the 1-D cases, the most computationally expensive WSGG calculations were the most complicated test cases (i.e., cases 2, 3 and 5), where RTE was solved for 2500 gray gases coupling the WSGG models of five different species via the superposition rule. To examine the efficiency of the present models, the CPU time of each test case was compared to the gray solution via a ratio defined as

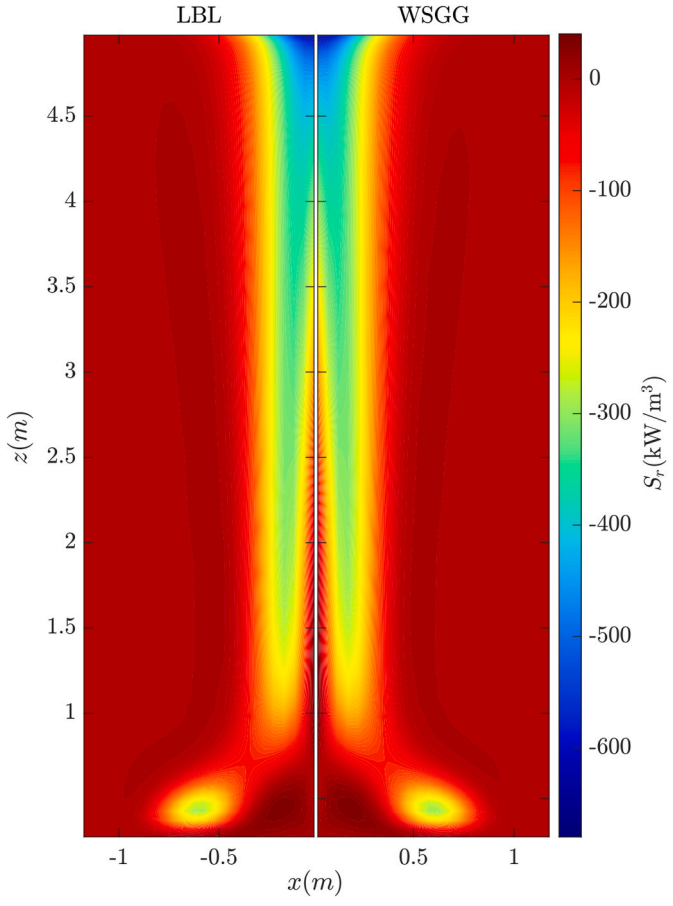

Fig. 15. Comparison of radiative heat source obtained from LBL integration and WSGG model in the 3-D validation case.

$$\text{CPU time} = \frac{t_{WSGG}}{t_{GG}} \tag{39}$$

where t_{WSGG} and t_{GG} are the CPU times of WSGG modeling and the gray solution, respectively. The values of the CPU times for each case are presented in Table 2. This table indicates that in case 2 onward where the superposition method was used, the CPU time of the WSGG solution has increased due to the larger number of the needed RTE solutions. The comparison presented in case 4 showed that with a very slight increment in errors, the WSGG model of premixed gases, namely H_2O–CO_2, could be combined with other gases which considerably decreases the number of gray gases and consequently lowers the computational time. Comparing the accuracies of the presented gray solutions with those of WSGG models, as expected, we see large errors. It is worth noting that case 1, in which the CPU cost of the gray model is evaluated, includes soot only which causes the case to behave more like a gray medium and therefore the WSGG model does not show its best privilege in terms of accuracy compared to the gray model. The computations of the present work were conducted using a computer with a Core i7-10750H CPU @ 2.60 GHz and 16 GB RAM and t_{GG} for the 1-D and 3-D cases were 0.012 s and 3.8 s, respectively.

5. Conclusion and remarks

This research presented new WSGG models for six different hydrocarbon fuel vapors, CO and soot. The new WSGG models include 4 gray gases plus one transparent gas and use fifth-order polynomials to describe the temperature dependency of the weighting functions. The accuracy of the proposed coefficients was evaluated through comparison of total emissivity of WSGG and LBL calculations. Moreover, they are further validated by being applied to several benchmarks including one-dimensional and three-dimensional cases. The predictions of the present WSGG models for radiative heat flux and heat source was compared to those of LBL integration method obtained by implementing high resolution absorption spectra. The benchmarks represented various level of inhomogeneity of temperature and species' concentrations in the medium. In the most complex 1-D case, a full combustion scenario containing inhomogeneous distributions of fuel gas, H_2O, CO_2, CO and soot in the gaseous medium were included. Additionally, the complete combustion of Methane was studied separately to show the performance of the WSGG model in the absence of CO and soot. Furthermore, the three-dimensional case confirmed the application of the WSGG models in a real fire scenario. In all the validation cases, the present novel WSGG models exhibited a good performance in both terms of accuracy and computational time. Accordingly, the contributions of this work are summarized by followings:

1) Using the high resolution experimental spectral absorption data of Wakatsuki [40] with a resolution of 0.5 cm^{-1}, new WSGG models were developed for vaporized Heptane, Methane, Methanol, MMA, Propane, Propylene, and Toluene with temperature of 300–1400K. They are totally new to the literature of thermal radiation and provide an efficient and accurate way for emissivity calculations of these gases in various temperatures and pathlengths. More importantly, they provide an efficient way to account for the non-gray effect of these gases in overall radiation heat transfer of combustion systems.
2) New WSGG models were presented for CH_4 and CO using the absorption spectra obtained from LBL calculations by implementing HITRAN 2008 and HITEMP2010 databases.
3) A new WSGG model was developed for soot at 300–3000K by implementing the correlations of Chang and Charalampopoulos [33] for spectral complex index of soot within the Rayleigh theory. The new model provides better performance over previous WSGG coefficients proposed for soot. Using the same data of spectral absorption coefficient of soot, a simple correlation is reported for the

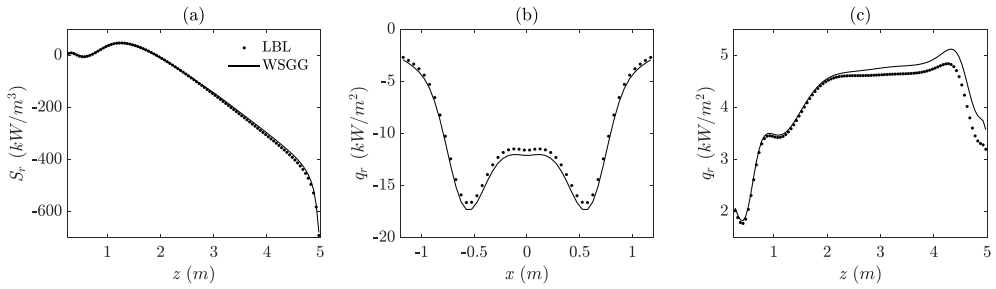

Fig. 16. Comparison of (a) radiative heat source on the centerline, (b) radiative heat flux on the pool surface and (c) radiative heat flux on the center line of the right side wall obtained by the LBL integration, the present WSGG models in the 3-D validation case.

Planck-mean absorption coefficient of soot for gray calculations. In most of the cases, especially with moderate to high soot load, a gray assumption for soot showed sufficient accuracy.

4) To demonstrate the application of the present models, the superposition rule for coupling different WSGG models was implemented and the computational performance of combining the new WSGG models with the previously published WSGG models for CO_2–H_2O mixture was addressed. Using a superposition approach for all the individual active species drastically increases the number of required RTE solutions and therefore CPU costs. It may not affordable for large engineering combustion systems. Nonetheless, coupling new WSGG models of fuel vapors with those presented previously for CO_2–H_2O mixture and considering soot as a gray medium can reduce the number of required RTE solutions in the superposition approach and therefore is recommended. It greatly speeded up the calculations while the average accuracy loss was generally less than 5%.

CRediT authorship contribution statement

Hosein Sadeghi: Methodology, Software, Validation, Formal analysis, Investigation, Resources, Data curation, Writing – original draft, Visualization. **Simo Hostikka:** Conceptualization, Methodology, Resources, Writing – review & editing, Supervision, Project administration, Funding acquisition. **Guilherme Crivelli Fraga:** Software, Validation, Formal analysis, Investigation, Writing – review & editing, Visualization. **Hadi Bordbar:** Conceptualization, Methodology, Software, Resources, Writing – review & editing, Investigation, Supervision, Project administration.

Declaration of competing interest

Reffering to manuscript entitled as "**Weighted-sum-of-gray-gases models for non-gray thermal radiation of hydrocarbon fuel vapors, CH4, CO and soot**", we wish to confirm that there are no known conflicts of interest associated with this publication and there has been no significant financial support for this work that could have influenced its outcome. We confirm that the manuscript has been read and approved by all named authors and that there are no other persons who satisfied the criteria for authorship but are not listed. We further confirm that the order of authors listed in the manuscript has been approved by all of us. We confirm that we have given due consideration to the protection of intellectual property associated with this work and that there are no impediments to publication, including the timing of publication, with respect to intellectual property. In so doing we confirm that we have followed the regulations of our institutions concerning intellectual property. We understand that the Corresponding Author is the sole contact for the Editorial process (including Editorial Manager and direct communications with the office). He is responsible for communicating with the other authors about progress, submissions of revisions and final approval of proofs. We confirm that we have provided a current, correct email address which is accessible by the Corresponding Author.

Acknowledgment

The authors greatly acknowledge the support of the Academy of Finland under grant No. 314487 and the Finnish Fire Protection Fund (Palosuojelurahasto). They also thank Dr. Kaoru Wakatsuki of Shinshu University for providing the experimental spectral absorption data of the fuel gases.

Appendix A. Supplementary data

Supplementary data to this article can be found online at https://doi.org/10.1016/j.firesaf.2021.103420.

Appendix B. The obtained WSGG model coefficients

The WSGG coefficients obtained for different fuel gases, CO and soot are reported in Tables B1–B9.

Table B1
The WSGG model coefficients for Heptane

j	$\kappa_{pj}(\mathrm{atm}^{-1}\mathrm{m}^{-1})$	b_{j0}	b_{j1}	b_{j2}	b_{j3}	b_{j4}	b_{j5}
1	1.5370	-7.2135×10^{-2}	7.8347×10^{-1}	−2.6215	4.0712	−3.0270	8.7282×10^{-1}
2	3.6421×10^{1}	-1.0995×10^{-2}	-5.2129×10^{-1}	5.1012	-1.1597×10^{1}	1.0527×10^{1}	−3.4280
3	2.0309×10^{2}	-9.1656×10^{-2}	9.7741×10^{-1}	−3.0661	5.1726	−4.3797	1.4266
4	1.0552×10^{1}	-1.8973×10^{-1}	1.9247×10^{-1}	−5.7570	8.5436	−6.3066	1.8305

Table B2
The WSGG model coefficients for Methane

j	$\kappa_{pj}(\mathrm{atm}^{-1}\mathrm{m}^{-1})$	b_{j0}	b_{j1}	b_{j2}	b_{j3}	b_{j4}	b_{j5}
1	1.6352×10^{-1}	-2.5429×10^{-1}	1.8623	−1.0442	−1.4615	1.5196	-3.7806×10^{-1}
2	1.7250×10^{1}	-1.4355×10^{-1}	1.2361	−2.5390	2.2398	-9.2219×10^{-1}	1.4638×10^{-1}
3	1.2668×10^{2}	-1.2161×10^{-2}	2.7405×10^{-1}	-7.3582×10^{-1}	7.7714×10^{-1}	-3.6778×10^{-1}	6.5290×10^{-2}
4	2.3385	-2.4021×10^{-1}	1.8795	−3.2156	2.2964	-7.3711×10^{-1}	8.5605×10^{-2}

Table B3
The WSGG model coefficients for Methanol

j	$\kappa_{pj}(\mathrm{atm}^{-1}\mathrm{m}^{-1})$	b_{j0}	b_{j1}	b_{j2}	b_{j3}	b_{j4}	b_{j5}
1	8.8782×10^{-1}	-8.0570×10^{-1}	9.3065	-3.5664×10^{1}	6.1553×10^{1}	-4.9448×10^{1}	1.5073×10^{1}
2	4.8043×10^{1}	-1.6725×10^{-1}	2.2709	−6.9218	1.4289×10^{1}	-1.5321×10^{1}	6.0186
3	3.6315×10^{2}	-8.4146×10^{-2}	1.4266	−4.5617	6.0885	−3.6752	8.1627×10^{-1}
4	1.0724×10^{1}	-5.3521×10^{-1}	4.1538	−5.8363	−3.4190	1.1388×10^{1}	−5.6415

Table B4
The WSGG model coefficients for MMA

j	$\kappa_{pj}(\mathrm{atm}^{-1}\mathrm{m}^{-1})$	b_{j0}	b_{j1}	b_{j2}	b_{j3}	b_{j4}	b_{j5}
1	8.8704×10^{-1}	2.9493×10^{-1}	−2.0848	7.3177	-1.2811×10^{1}	1.0668×10^{1}	−3.3742
2	3.9451×10^{1}	-8.9431×10^{-1}	9.2090	-2.9388×10^{1}	4.6127×10^{1}	-3.5605×10^{1}	1.0702×10^{1}
3	1.9847×10^{2}	-4.2836×10^{-1}	5.3939	-1.4825×10^{1}	1.6010×10^{1}	−6.6940	5.6874×10^{-1}
4	7.7937	-5.2268×10^{-1}	5.0183	-1.5707×10^{1}	2.5272×10^{1}	-2.0392×10^{1}	6.4346

Table B5
The WSGG model coefficients for Propane

j	$\kappa_{pj}(\mathrm{atm}^{-1}\mathrm{m}^{-1})$	b_{j0}	b_{j1}	b_{j2}	b_{j3}	b_{j4}	b_{j5}
1	9.0342×10^{-1}	4.0493×10^{-1}	−2.8307	8.4037	-1.2895×10^{1}	1.0320×10^{1}	−3.3724
2	2.9729×10^{1}	-2.7372×10^{-1}	2.4634	−5.5543	5.2753	−1.8980	5.4603×10^{-2}
3	1.7891×10^{2}	2.4708×10^{-2}	-1.2564×10^{-1}	1.9339×10^{-1}	6.7240×10^{-1}	−1.4062	6.7638×10^{-1}
4	6.7645	-7.6421×10^{-1}	6.3217	-1.7276×10^{1}	2.4754×10^{1}	-1.8816×10^{1}	5.8805

Table B6
The WSGG model coefficients for Propylene

j	$\kappa_{pj}(\mathrm{atm}^{-1}\mathrm{m}^{-1})$	b_{j0}	b_{j1}	b_{j2}	b_{j3}	b_{j4}	b_{j5}
1	7.4676×10^{-1}	-8.3629×10^{-1}	8.5443	-2.7740×10^{1}	4.0924×10^{1}	-2.8509×10^{1}	7.6318
2	2.8174×10^{1}	−1.0268	9.1590	-2.4929×10^{1}	3.0986×10^{1}	-1.8302×10^{1}	4.1608
3	1.1871×10^{2}	2.4668×10^{-1}	-1.1281×10^{-2}	−3.5468	8.7861	−8.1240	2.6538
4	5.8714	8.1020×10^{-2}	−1.0218	6.7291	-1.3141×10^{1}	1.0272×10^{1}	−2.8401

Table B7
The WSGG model coefficients for Toluene

j	$\kappa_{pj}(\mathrm{atm}^{-1}\mathrm{m}^{-1})$	b_{j0}	b_{j1}	b_{j2}	b_{j3}	b_{j4}	b_{j5}
1	1.0561	−1.7092	2.0121×10^{1}	-8.0686×10^{1}	1.4556×10^{2}	-1.2147×10^{2}	3.8226×10^{1}
2	4.1888×10^{1}	2.7170×10^{-1}	−3.5907	1.9529×10^{1}	-4.0309×10^{1}	3.5981×10^{1}	-1.1782×10^{1}
3	2.7454×10^{2}	9.6399×10^{-3}	6.7764×10^{-1}	-3.1934	5.6735	−4.5133	1.3530
4	1.0422×10^{1}	6.7483×10^{-1}	−9.4967	4.8507×10^{1}	-9.8544×10^{1}	8.7479×10^{1}	-2.8508×10^{1}

Table B8
The WSGG model coefficients for CO

j	$\kappa_{pj}(\mathrm{atm}^{-1}\mathrm{m}^{-1})$	b_{j0}	b_{j1}	b_{j2}	b_{j3}	b_{j4}	b_{j5}
1	1.7920×10^{-1}	-5.3582×10^{-3}	-1.4397×10^{-3}	4.0604×10^{-1}	-5.7254×10^{-1}	2.8282×10^{-1}	-4.7820×10^{-2}
2	1.2953×10^{1}	-5.7642×10^{-2}	4.2020×10^{-1}	-7.6297×10^{-1}	6.0302×10^{-1}	-2.2181×10^{-1}	-3.1122×10^{-2}
3	1.2900×10^{2}	-1.6152×10^{-2}	1.2220×10^{-1}	-2.2207×10^{-1}	1.7430×10^{-1}	-6.3464×10^{-2}	8.8012×10^{-3}
4	1.7918	-6.7961×10^{-2}	4.2204×10^{-1}	-5.4894×10^{-1}	2.8819×10^{-1}	-6.2318×10^{-2}	3.7321×10^{-3}

Table B9
The WSGG model coefficients for soot

j	$\kappa_{f,j}(\mathrm{m}^{-1})$	b_{j0}	b_{j1}	b_{j2}	b_{j3}	b_{j4}	b_{j5}
1	1.4530×10^{5}	1.8613	−7.7857	1.2809×10^{1}	-1.0158×10^{1}	3.8717	-5.6880×10^{-1}
2	2.0836×10^{6}	2.5975×10^{-1}	−2.9708	9.6830	−9.7681	4.1073	-6.3057×10^{-1}
3	7.5475×10^{5}	−1.1374	1.0625×10^{1}	-2.1665×10^{1}	1.8750×10^{1}	−7.4578	1.1219
4	4.2113×10^{6}	-3.8367×10^{-2}	4.2159×10^{-1}	-1.4101	1.7225	-7.5889×10^{-1}	1.1454×10^{-1}

References

[1] M.F. Modest, in: Radiative Heat Transfer, third ed., Academic press, 2013.
[2] J. Consalvi, F. Liu, A database of narrow-band parameters for fuels commonly encountered in fire applications,, Fire Saf. J. 78 (2015) 202–218, https://doi.org/10.1016/j.firesaf.2015.10.002.
[3] M.H. Bordbar, G. Wecel, T. Hyppänen, A line by line based weighted sum of gray gases model for inhomogeneous CO2–H2O mixture in oxy-fired combustion, Combust. Flame 161 (9) (2014) 2435–2445, https://doi.org/10.1016/j.combustflame.2014.03.013.
[4] G. C. Fraga, H. Bordbar, S. Hostikka, F. H. R. França, Benchmark solutions of three-dimensional radiative transfer in nongray media using line-by-line integration, J. Heat Tran. 142(3). doi:10.1115/1.4045666.
[5] B.W. Webb, V.P. Solovjov, F. André, Chapter four - the spectral line weighted-sum-of-gray-gases (slw) model for prediction of radiative transfer in molecular gases, in: E.M. Sparrow, J.P. Abraham, J.M. Gorman, W. Minkowycz (Eds.), Advances in Heat Transfer 51, Elsevier, 2019, pp. 207–298, https://doi.org/10.1016/bs.aiht.2019.08.003, of Advances in Heat Transfer.
[6] V.P. Solovjov, B.W. Webb, F. André, D. Lemonnier, Locally correlated slw model for prediction of gas radiation in non-uniform media and its relationship to other global methods, J. Quant. Spectrosc. Radiat. Transf. 245 (2020), 106857, https://doi.org/10.1016/j.jqsrt.2020.106857.
[7] L. Pierrot, P. Rivière, A. Soufiani, J. Taine, A fictitious-gas-based absorption distribution function global model for radiative transfer in hot gases,, J. Quant. Spectrosc. Radiat. Transf. 62 (5) (1999) 609–624, https://doi.org/10.1016/S0022-4073(98) 00124–1.
[8] C. Wang, M.F. Modest, T. Ren, J. Cai, B. He, Comparison and refinement of the various full-spectrum k-distribution and spectral line weighted-sum-of-gray-gases models for nonhomogeneous media, J. Quant. Spectrosc. Radiat. Transf. 271 (2021), 107695, https://doi.org/10.1016/j.jqsrt.2021.107695.
[9] M.F. Modest, The Weighted-Sum-Of-Gray-Gases Model for Arbitrary Solution Methods in Radiative Transfer. https://doi.org/10.1115/1.2910614.
[10] H. Hottel, A. Sarofim, Radiative Transport, McCravv Hill, New York.
[11] M.H. Bordbar, T. Hyppänen, The correlation based zonal method and its application to the back pass channel of oxy/air-fired CFB boiler, Appl. Therm. Eng. 78 (2015) 351–363, https://doi.org/10.1016/j.applthermaleng.2014.12.046.
[12] T. Smith, Z. Shen, J. Friedman, Evaluation of Coefficients for the Weighted Sum of Gray Gases Model. https://doi.org/10.1115/1.3245174.
[13] L.J. Dorigon, G. Duciak, R. Brittes, F. Cassol, M. Galarca, F.H. França, WSGG correlations based on hitemp2010 for computation of thermal radiation in non-isothermal, non-homogeneous H2O/CO2 mixtures, Int. J. Heat Mass Tran. 64 (2013) 863–873, https://doi.org/10.1016/j.ijheatmasstransfer.2013.05.010.
[14] T. Kangwanpongpan, F.H. França, R.C. da Silva, P.S. Schneider, H.J. Krautz, New correlations for the weighted-sum-of-gray-gases model in oxy-fuel conditions based on HITEMP 2010 database, Int. J. Heat Mass Tran. 55 (25–26) (2012) 7419–7433, https://doi.org/10.1016/j.ijheatmasstransfer.2012.07.032.
[15] R. Johansson, B. Leckner, K. Andersson, F. Johnsson, Account for variations in the H2O to CO2 molar ratio when modelling gaseous radiative heat transfer with the weighted-sum-of-grey-gases model, Combust. Flame 158 (5) (2011) 893–901, https://doi.org/10.1016/j.combustflame.2011.02.001.
[16] C. Yin, L.C. Johansen, L.A. Rosendahl, S.K. Kær, New weighted sum of gray gases model applicable to computational fluid dynamics (CFD) modeling of oxy- fuel combustion: derivation, validation, and implementation, Energy & Fuels 24 (12) (2010) 6275–6282, https://doi.org/10.1021/ef101211p.
[17] F.R. Coelho, F.H. França, WSGG correlations based on hitemp2010 for gas mixtures of H2O and CO2 in high total pressure conditions, Int. J. Heat Mass Tran. 127 (2018) 105–114, https://doi.org/10.1016/j.ijheatmasstransfer.2018.07.075.
[18] H. Bordbar, F.R. Coelho, G.C. Fraga, F.H. França, S. Hostikka, Pressure-dependent weighted-sum-of-gray-gases models for heterogeneous CO2-H2O mixtures at sub- and super-atmospheric pressure, Int. J. Heat Mass Tran. 173 (2021), 121207, https://doi.org/10.1016/j.ijheatmasstransfer.2021.121207.
[19] V. Kez, F. Liu, J. Consalvi, J. Ströhle, B. Epple, A comprehensive evaluation of different radiation models in a gas turbine combustor under conditions of oxy-fuel combustion with dry recycle,, J. Quant. Spectrosc. Radiat. Transf. 172 (2016) 121–133, https://doi.org/10.1016/j.jqsrt.2015.11.002.
[20] V. Kez, J. Consalvi, F. Liu, J. Ströhle, B. Epple, Assessment of several gas radiation models for radiative heat transfer calculations in a three-dimensional oxy-fuel furnace under coal-fired conditions, Int. J. Therm. Sci. 120 (2017) 289–302, https://doi.org/10.1016/j.ijthermalsci.2017.06.017.
[21] V. Kez, J.-L. Consalvi, F. Liu, M. Koch, O. Hatzfeld, R. Kneer, Development of a weighted-sum-of-gray-gases model for modeling radiative heat transfer in coal-fired oxy-fuel boilers, in: Proceedings of the 9th International Symposium on Radiative Transfer, RAD-19, Begel House Inc, 2019.
[22] X. Yang, Z. He, S. Dong, H. Tan, Evaluation of the non-gray weighted sum of gray gases models for radiative heat transfer in realistic non-isothermal and non-homogeneous flames using decoupled and coupled calculations, Int. J. Heat Mass Tran. 134 (2019) 226–236, https://doi.org/10.1016/j.ijheatmasstransfer.2019.01.038.
[23] L. Pierrot, A. Soufiani, J. Taine, Accuracy of narrow-band and global models for radiative transfer in H2O, CO2, and H2O-CO2 mixtures at high temperature, J. Quant. Spectrosc. Radiat. Transf. 62 (5) (1999) 523–548, https://doi.org/10.1016/S0022-4073(98) 00125–3.
[24] J. Cai, M.F. Modest, Improved full-spectrum k-distribution implementation for inhomogeneous media using a narrow-band database, J. Quant. Spectrosc. Radiat. Transf. 141 (2014) 65–72, https://doi.org/10.1016/j.jqsrt.2014.02.028.
[25] J. Badger, B. Webb, V. Solovjov, An exploration of advanced SLW modeling approaches in comprehensive combustion predictions, Combust. Sci. Technol. (2019) 1–17, https://doi.org/10.1080/00102202.2019.1678907, doi:.
[26] J. Consalvi, F. Andre, F. Coelho, F. Franca, F. Nmira, M. Galtier, V. Solovjov, B. Webb, Assessment of engineering gas radiative property models in high pressure turbulent jet diffusion flames, J. Quant. Spectrosc. Radiat. Transf. 253 (2020), 107169, https://doi.org/10.1016/j.jqsrt.2020.107169.
[27] V.P. Solovjov, B.W. Webb, F. Andre, The rank correlated FSK model for prediction of gas radiation in non-uniform media, and its relationship to the rank correlated SLW model, J. Quant. Spectrosc. Radiat. Transf. 214 (2018) 120–132, https://doi.org/10.1016/j.jqsrt.2018.04.026.
[28] F. Cassol, R. Brittes, F.H. França, O.A. Ezekoye, Application of the weighted-sum-of-gray-gases model for media composed of arbitrary concentrations of H2O, CO2 and soot, Int. J. Heat Mass Tran. 79 (2014) 796–806, https://doi.org/10.1016/j.ijheatmasstransfer.2014.08.032.
[29] Y. Zhou, C. Wang, T. Ren, A machine learning based efficient and compact full-spectrum correlated *k*-distribution model, J. Quant. Spectrosc. Radiat. Transf. 254 (2020), 107199, https://doi.org/10.1016/j.jqsrt.2020.107199.
[30] L.G.P. Rodrigues, I.M. Machado, A. Ziemniczak, F.M. Pereira, P.R. Pagot, F.H. R. França, Comparisons between numerical simulations and experimental

measurements of radiative heat flux for a series of ch4/n2 diluted laminar non-premixed flames, Combust. Sci. Technol. 193 (1) (2021) 1–22, https://doi.org/10.1080/00102202.2019.1646733, doi:.
[31] André F., Coelho F., Consalvi J-L., Franca F. H. R., Galtier M., et al.. Accuracy of engineering methods for radiative transfer in co2-h2o mixtures at high temperature, in: Proceedings of the 9th International Symposium on Radiative Transfer, RAD-19, Begel House Inc. DOI: 10.1615/RAD-19.500.
[32] N. Bressloff, The influence of soot loading on weighted sum of grey gases solutions to the radiative transfer equation across mixtures of gases and soot,, Int. J. Heat Mass Tran. 42 (18) (1999) 3469–3480, https://doi.org/10.1016/S0017-9310(99)00031–00039.
[33] H.-c. Chang, T. Charalampopoulos, Determination of the wavelength dependence of refractive indices of flame soot, Proceedings of the Royal Society of London, Series A: Mathematical and Physical Sciences 430 (1990) (1880) 577–591, https://doi.org/10.1098/rspa.1990.0107.
[34] R. Brittes, F. Roman Centeno, A. Ziemniczak, F. Franca, et al., WSGG model correlations to compute nongray radiation from carbon monoxide in combustion applications, J. Heat Tran. 139(4). doi:https://doi.org/10.1115/1.4035394.
[35] K. Wakatsuki, G.S. Jackson, J. Kim, A. Hamins, M.R. Nyden, S.P. Fuss, Determination of planck mean absorption coefficients for hydrocarbon fuels, Combust. Sci. Technol. 180 (4) (2008) 616–630, https://doi.org/10.1080/00102200701838941, doi:.
[36] J. Consalvi, F. Liu, Radiative heat transfer in the core of axisymmetric pool fires–i: evaluation of approximate radiative property models, Int. J. Therm. Sci. 84 (2014) 104–117, https://doi.org/10.1016/j.ijthermalsci.2014.04.018.
[37] J. Consalvi, F. Liu, Radiative heat transfer through the fuel-rich core of laboratory-scale pool fires, Combust. Sci. Technol. 186 (4–5) (2014) 475–489, https://doi.org/10.1080/00102202.2014.883221.
[38] F. Alinejad, H. Bordbar, S. Hostikka, Development of full spectrum correlated k-model for spectral radiation penetration within liquid fuels, Int. J. Heat Mass Tran. 158 (2020), 119990, https://doi.org/10.1016/j.ijheatmasstransfer.2020.119990.
[39] F. Alinejad, H. Bordbar, S. Hostikka, Improving the modeling of spectral radiation penetration into the condensed materials with the separated full spectrum correlated-k method, Int. J. Heat Mass Tran. (2021), 121448.
[40] K. Wakatsuki, High Temperature Radiation Absorption of Fuel Molecules and an Evaluation of its Influence on Pool Fire Modeling, 2005. Ph.D. thesis.
[41] F. R. Coelho, G. C. Fraga, F. H. R. Franca, Generation of new wsgg correlations and analysis on the importance of considering transparent windows for soot.
[42] M.K. Denison, B.W. Webb, A Spectral Line-Based Weighted-Sum-Of-Gray-Gases Model for Arbitrary RTE Solvers. https://doi.org/10.1115/1.2911354.
[43] H. Bordbar, S. Hostikka, Numerical solution of LBL spectral radiation of a n-heptane pool fire, in: Proceedings of the 9th International Symposium on Radiative Transfer, RAD-19, Begel House Inc, 2019, https://doi.org/10.1615/RAD-19.80.
[44] H. Bordbar, S. Hostikka, P. Boulet, G. Parent, Numerically resolved line by line radiation spectrum of large kerosene pool fires, J. Quant. Spectrosc. Radiat. Transf. 254 (2020), 107229, https://doi.org/10.1016/j.jqsrt.2020.107229.
[45] K. Wakatsuki, S. Fuss, A. Hamins, M. Nyden, A technique for extrapolating absorption coefficient measurements to high temperatures, Proc. Combust. Inst. 30 (1) (2005) 1565–1573, https://doi.org/10.1016/j.proci.2004.08.078.
[46] L. Rothman, I. Gordon, R. Barber, H. Dothe, R. Gamache, A. Goldman, V. Perevalov, S. Tashkun, J. Tennyson, HITEMP, the high-temperature molecular spectroscopic database, J. Quant. Spectrosc. Radiat. Transf. 111 (15) (2010) 2139–2150, https://doi.org/10.1016/j.jqsrt.2010.05.001.
[47] L.S. Rothman, I.E. Gordon, A. Barbe, D.C. Benner, P.F. Bernath, M. Birk, V. Boudon, L.R. Brown, A. Campargue, J.-P. Champion, et al., The HITRAN 2008 molecular spectroscopic database, J. Quant. Spectrosc. Radiat. Transf. 110 (9–10) (2009) 533–572, https://doi.org/10.1016/j.jqsrt.2009.02.013.
[48] H. Chu, F. Liu, H. Zhou, Calculations of gas thermal radiation transfer in one-dimensional planar enclosure using LBL and SNB models, Int. J. Heat Mass Tran. 54 (21–22) (2011) 4736–4745, https://doi.org/10.1016/j.ijheatmasstransfer.2011.06.002.
[49] H. Bordbar, T. Hyppänen, Line by line based band identification for non-gray gas modeling with a banded approach, Int. J. Heat Mass Tran. 127 (2018) 870–884, https://doi.org/10.1016/j.ijheatmasstransfer.2018.06.093.
[50] R. Johansson, K. Andersson, B. Leckner, H. Thunman, Models for gaseous radiative heat transfer applied to oxy-fuel conditions in boilers, Int. J. Heat Mass Tran. 53 (1) (2010) 220–230, https://doi.org/10.1016/j.ijheatmasstransfer.2009.09.039.
[51] H. Bordbar, G.C. Fraga, S. Hostikka, An extended weighted-sum-of-gray-gases model to account for all CO2-H2O molar fraction ratios in thermal radiation, Int. Commun. Heat Mass Tran. 110 (2020), 104400, https://doi.org/10.1016/j.icheatmasstransfer.2019.104400.
[52] A.A. Lacis, V. Oinas, A description of the correlated k distribution method for modeling nongray gaseous absorption, thermal emission, and multiple scattering in vertically inhomogeneous atmospheres, arXiv:https://agupubs.onlinelibrary.wiley.com/doi/pdf/10.1029/90JD01945, J. Geophys. Res.: Atmosphere 96 (D5) (1991) 9027–9063, https://doi.org/10.1029/90JD01945.
[53] M.H. Bordbar, T. Hyppänen, Multiscale numerical simulation of radiation heat transfer in participating media, Heat Transf. Eng. 34 (1) (2013) 54–69, https://doi.org/10.1080/01457632.2013.695210.